

# Aeromechanical Analysis of a Smart Helicopter Rotor in Forward Flight

Jacopo Serafini<sup>\*1</sup>, Claudio Testa<sup>\*\*2</sup>, Stefania Leone<sup>\*\*3</sup>

<sup>\*1</sup> Department of Engineering, University Roma Tre, Rome, Italy 00146

<sup>\*\*2 & 3</sup> CNR-INSEAN Italian Ship Model Basin, Rome, Italy, 00128

<sup>\*1</sup> [serafini@uniroma3.it](mailto:serafini@uniroma3.it)

<sup>\*\*2</sup> [claudio.testa@cnr.it](mailto:claudio.testa@cnr.it)

<sup>\*\*3</sup> [leone-ste@hotmail.it](mailto:leone-ste@hotmail.it)

**ABSTRACT** – This paper deals with a smart system integrated into a helicopter blade aimed at giving an anhedral shape to the blade tip region to alleviate the blade-vortex interaction phenomenon that may cause reduced helicopter performance in terms of noise and vibrations. The blade tip morphing is obtained through the joint action of a magneto-rheological fluid (MRF) device, a shape-memory alloy ribbons-based (SMA) device and a set of concentrated masses properly distributed spanwise. The presence of this smart actuator (particularly the concentrated masses) inside the blades modifies the aeromechanical behaviour of the rotor and may be detrimental in terms of hub vibratory loads, pitch control effectiveness and aeroelastic stability. Following a previous literature work concerning with the effectiveness of the smart actuated rotor in hovering conditions, the present paper focuses on the aeromechanical effects due to the inclusion of the smart device in a four-bladed helicopter rotor in forward flight where blade morphing is not needed. Aim of this work is to investigate on the compatibility of the smart system with the required aeromechanical performance of the rotor, highlighting the feasibility of its application on helicopters.

**Keywords:** Smart structures, Blade morphing, Anhedral blade, Aeroelasticity

## 1. INTRODUCTION

The evaluation of noise generated by rotating blades is one of the most important issues related to helicopter performance and acoustic certification. Since the first half of the 90's, the interest of the rotorcraft researchers community has been focused on the assessment and improvement of numerical tools able to predict the pressure disturbance in the flow-field and, at the same time, on the development and manufacture of integrated systems to reduce it. As a matter of fact, the complexity of rotating blades aeromechanics makes this task very difficult; the high energy levels and the significant displacements, forces and moments involved, make unpractical some engineering solutions based on smart materials integrated into the rotor system which would guarantee light-weight and adaptivity. Hence, in spite of the availability of different strategies based on current technologies for reducing noise and vibration, their practical application is currently limited to few approaches. Several phenomena are involved into sound generation by helicopter rotor: among them, the Blade Vortex Interaction (BVI) producing extremely annoying impulsive noise is object of extensive theoretical and experimental research. BVI occurs when strong tip vortices, dominating the rotor wake, impinge or pass close to the rotor blades, thus producing impulsive changes of the blade loads and, in turn, high noise and vibration levels. It is well documented [1] that the interaction of the tip vortex with the following blade concerns mainly the descent flight at relatively low speed (or the hover condition, for particular blade geometry); this leads to a strong resistance to the widespread operation of helicopters in densely populated areas. Moreover, the induced vibrations increase pilot workload, reduce component fatigue life and increase maintenance costs. A possible strategy to alleviate BVI noise is to diffuse the blade tip vortex, or displace it far away from the following blades by increasing the blade vortex miss-distance. Such a solution may be achieved through an anhedral tip shape; previous research [2], [3] has shown that typically tip vortices involved in BVI are related to the 10 – 15% tip blade portion and noise is attained if a mean blade slope variation of 5°, at least, is achieved. A drawback in following this noise alleviation strategy is that the actuation power provided by any actuator device is usually not enough to bend the tip region for achieving an anhedral shape; in fact, nowadays, there not exist smart rotors able to morph their blades during the descent flight phase since the anhedral shape may be assured only during the blade manufacturing process. Some of the authors have faced the problem of transforming the blade tip to get an anhedral shape [4], [5] showing that in principle the blade morphing may be achieved by exploiting the energy of the centrifugal field and not only through the actions provided by conventional actuators based on piezoelectric materials (PZT), shape-memory alloys (SMA), etc. In those papers, an innovative integrated smart stiffness-variable system is proposed and a feasibility study is addressed to investigate its potentiality. The aforementioned smart architecture is composed of three different and fully integrated sub-systems: a magneto-rheological fluid (MRF) device, a shape-memory alloy ribbons (SMA) device and a set concentrated masses, properly distributed spanwise. Task of the MRF system is to reduce the blade stiffness in the controlled zone;

once it is switched on, the bending moments provided by eccentric masses (properly located inside the blade box) and the actions by the SMA actuators, morph the blade tip. As shown in Refs [5], [6], the spanwise mass distribution yields the main contribution for achieving the anhedral shape, whereas the SMA actuator allow to mould the shape for obtaining the characteristic beak profile, typical of any anhedral configuration. Although by increasing the amount of concentrated masses, a higher morphing action is expected, the choice of masses, bending-stiffness reduction and SMA-wires strength has to be a compromise yielding a trimmed-stable rotor, along with limited vibration levels for all flight conditions. A numerical investigation on the aeroelastic behaviour of the proposed smart rotor has been performed in Ref. [6] for a hovering condition; it shows that the range of mass values allowing blade morphing and aeroelastic stability does exist. Taking advantages from previous studies, the present work extends the investigation to forward flight conditions where, even if BVI does not occur, the presence of the concentrated masses in the non-actuated blades may play an important role in the aeromechanical behaviour of the rotor (hub loads, pitch control effectiveness and aeroelasticity). Aim of this work is the analysis of the compatibility between the smart system and aeromechanical rotor performance. For this purpose, the blade is modelled as an isotropic, elastic, non-uniform rotating beam undergoing lead-lag, flap and torsion displacements, whereas the aerodynamic loads are given by a strip-theory approach based a quasi-steady approximation of the Greenberg theory combined with a 3D free-wake aerodynamic solver providing the wake inflow on the rotor disk. The steady-periodic blade response is determined by coupling the equations of blade dynamics with the trim equations; then linearized equations for small perturbations are derived and the aeroelastic stability is examined through an eigenanalysis.

**2. ACTUATION SYSTEM PERFORMANCE IN HOVERING CONDITIONS**

For the sake of completeness, some of the most important features of the proposed actuation system and the guidelines obtained from previous studies are briefly outlined. More details are shown in [5], [6].

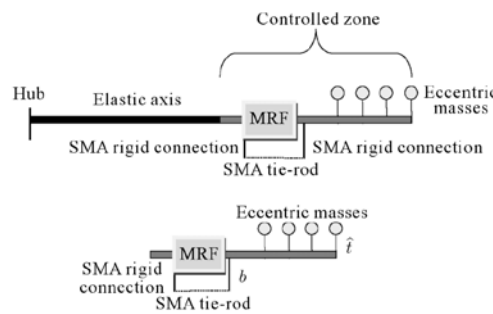


Fig. 1 Sketch of the smart system

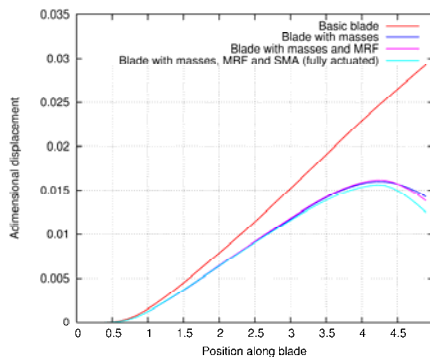


Fig. 2 Smart device effect on flapping displacement

The typical problem of any smart structure consists of preserving the necessary robustness with the addition of some liability to get the required shape. By combining the advantages of an adaptive-stiffness beam with the energy developed by rotation, an anhedral shape may be achieved. Note that the exploitation of the actuation forces coming from centrifugal loads represents an original way of facing the problem of adaptive structures for rotating blades. As mentioned above, the innovative smart architecture proposed in Refs [4], [5] is based on an on-off system composed of a MRF-SMA device and a set of concentrated masses properly distributed inside the blade box (see Fig.1). The MRF system provides a spanwise local control of the bending stiffness, whereas the SMA elements, combined with the forces induced by the concentrated masses, bend the structure. When the anhedral shape is needed the intensity of the magnetic field is decreased thus reducing the bending stiffness,

concentrated masses are suitably displaced and the SMA elements are switched on. In such a way, the joint bending actions of concentrated masses and SMA actuator deflect the blade tip region. Once the required anhedral shape is achieved, the magnetic field is increased until the configuration is frozen and then the SMA device is switched off. Differently, when no anhedral configuration is needed a magnetic field is applied to the MRF device so that the fluid viscosity increases and the blade controlled zone is completely locked. In this case the SMA tie-rod is switched off and masses are still located in their rest positions. In the following, the above actuation strategy is discussed and the role of the different device is shown to better understand the need of using their coupled actions. As highlighted in Refs [4], [5], if only the MRF device is applied, the geometrical blade configuration would remain very close to the non-actuated one even for a stiffness variation,  $K_{MRF}$ , equal to the 65% of the initial stiffness. However, for  $K_{MRF}$  equal to the 75% of the initial stiffness a slope variation  $\Delta\theta = -0.11^\circ$  is achieved between  $x = 0.9R$  and the blade tip ( $R$  denotes the blade radius). Note that the bending stiffness reduction is localized between  $a = 0.87R$  and  $b = 0.9R$  (see Fig.1); thus, only slight variations of the natural rotating frequencies appear. Differently, the investigation on the effects due only to the SMA actuator reveals that the corresponding flap bending moments have the capability to modify the structure. The best configuration is achieved when the maximum allowable number of ribbons (depending on the available blade box internal space) is used. For the blade considered in Ref. [6] having NACA 0015 airfoil sections, 30 ribbons, providing a 15 KN force, produce a slope variation  $\Delta\theta = -0.24^\circ$ . Coupling the MRF device with the SMA actuator, the advantages of local stiffness reduction are exploited. However, in this case, the weakening provided by the MRF cannot be too large: numerical investigations [5] have shown that for a realistic four-bladed rotor,  $K_{MRF}$  has not to be lower than the 50% of the initial stiffness to avoid transforming the blade tip into a real hinged-beam and experiencing too large blade tip displacements. Accounting for this constraint, the combined action of MRF and SMA yields  $\Delta\theta = -0.26^\circ$ . Nonetheless, the resulting blade tip shape does not match the required one even if the SMA device is applied at the maximum of its capability [5]. This problem may be overcome by exploiting the actions induced by the centrifugal fields. Indeed, by using a set of masses located above the elastic axis, the resulting bending moment induced by the centrifugal forces is able to modify the blade shape. As it is shown in Ref. [5] three masses are at least required (see Fig.1):  $m_1$  to improve the effect of the MRF-SMA device,  $m_2$  to allow moulding the blade shape and  $M$ , located at the blade tip, to modify the blade shape into the targeted anhedral configuration. Note that in the MRF-SMA based actuation system, shape-memory alloys are used to bend the outer portion of the blade, whereas, when concentrated masses are included, the major bending effect is due to the centrifugal field, with the SMA actuator providing local bending slope change in the area where the MRF device acts (thus, obtaining the characteristics beak profile). In details, by using  $m_1 = m_2 = 0.25 \text{ Kg}$  and  $M = 1.5 \text{ kg}$  (corresponding to a mass increase equal to the 8% of the blade mass), for  $K_{MRF}$  equal to the 50% of the initial stiffness and using 15 SMA ribbons, the bending slope variation obtained in Ref. [5] is  $\Delta\theta = -2.2^\circ$ , which corresponds to the 44% of the requirement (see Refs [2], [3]). This result could be improved by increasing the amount of concentrated masses or the SMA ribbons or decreasing the stiffness in the controlled zone. However, the satisfaction of the requirement was well beyond the scope of that investigation aimed at addressing a feasibility study on a realistic helicopter rotor to highlight capabilities and drawbacks of the proposed integrated system.

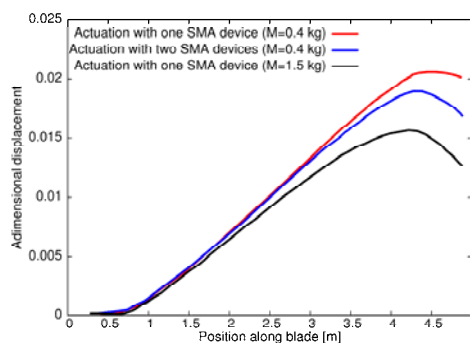


Fig. 3 Flap displacement due to one and two SMA actuators

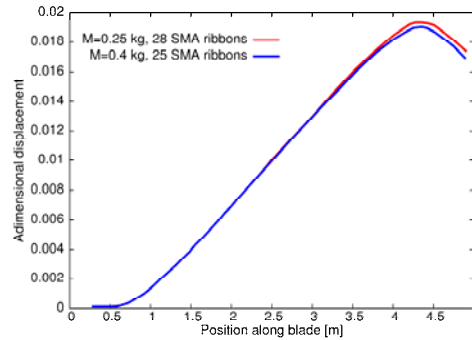


Fig. 4 Flap deformation due to two SMA actuators

After having shown the capability of the proposed integrated device system to change the shape of the blade tip region, the attention has been focused on the influence it may have on blade aeroelastic behaviour, particularly because of the presence of concentrated masses. For this reason, a further investigation [6] has considered the smart device applied to a Bo105-type four-bladed hingeless rotor with NACA 0015 cross-sections and rotational speed  $\Omega = 44 \text{ rad/s}$  [7], in hovering. The results of this analysis have proven that, for an efficient use of the smart system, the SMA actuator has to be positioned between  $0.87 R$  and  $0.92 R$ , while the MRF device between  $0.87 R$  and  $0.9 R$ . Indeed, by using 13 ribbons (providing a 6500 N force), imposing a bending stiffness reduction  $K_{\text{MRF}}$  equal to 50% of the initial stiffness and applying a concentrated masses configuration with  $M = 1.5 \text{ kg}$  and  $m_1 = m_2 = 0.5 \text{ kg}$ , a beak profile was obtained for the fully-actuated blade. The result in terms of flap displacement is shown in Fig.2. The amount of additional mass included in the above configuration does not overcome the 11% of the basic blade mass and is the result of an optimization study aimed to amplify the bending effect of the centrifugal field. However, blade tip morphing has to match both BVI noise abatement and requirements concerning rotor dynamic response. In particular, the modified dynamic response has to avoid blade resonances and aeroelastic instabilities within operative conditions. Unfortunately, the analysis of the above smart blade has shown that it is unstable and that the aeroelastic behaviour strongly depends on the value of the tip mass  $M$ , whilst the effect of  $m_1$  and  $m_2$  is almost negligible [6]. Numerical outcomes prove that aeroelastic stability is assured for  $M = 0.4 \text{ kg}$  (about 70% reduction) and  $m_1 = m_2 = 0.39 \text{ kg}$ . Since blade morphing induced-effects by such configuration is reduced, a second SMA actuator has been located close to the blade tip [6] to get a tip shape similar to that given by the higher-mass configuration. Through this actuation strategy, keeping  $m_1$  and  $m_2$  constant, the blade equilibrium configuration does not change for tip mass values between  $0.25 \text{ Kg}$  and  $0.4 \text{ Kg}$ . The SMA-based actuation device has to produce a 12500 N force (25 ribbons) when  $M = 0.4 \text{ kg}$ , while a 14000 N force (28 ribbons) is needed when  $M = 0.25 \text{ kg}$  [6]. Higher mass reduction is not allowed since 30 ribbons is approximately the maximum value for cross-sections typically used in conventional helicopter blades. Figures 3 and 4 summarize the above results. Finally, the aeroelastic analysis has shown that, for a rotor thrust  $T = 25000 \text{ N}$ , the re-designed actuated smarted rotor is stable for the tip mass range examined,  $0.25 \text{ kg} < M < 0.4 \text{ kg}$  [6].

### 3. NON-ACTUATED BLADE MODELLING IN FORWARD FLIGHT

In the following, the effects of the integrated morphing system on the aeroelastic behaviour of a smart rotor in forward flight are investigated. In this case, even though the system remains non-actuated (blade morphing is not needed), the effectiveness of pitch controls and increased vibrating hub loads may become possible additional critical issues due to the presence of concentrated masses.

#### A. BLADE AEROELASTICITY

Akin to the analysis of the hovering rotor, [6] the elastic blade model is based on the nonlinear flap-lag-torsion equations of motion presented in Ref. [8] and subsequently extended by some of the authors in [9], [10]. Rotor blades are modelled as long, straight, slender, non-homogeneous, isotropic beams; the theory herein used, is intended for moderate displacements, accurate to second order, and based on the hypothesis that squares of bending slopes, twist, thickness-radius and chord-radius ratios are small with respect to unity. Radial non-uniformities (mass, stiffness, etc.), chordwise offsets of the mass centroid and tension axes from the elastic axis, and precone are included; other details, such as blade root feathering flexibility, torque offset, blade sweep and droop are not considered. Eliminating the radial displacement from the set of equations by solving it in terms of local tension, the equations governing the aeroelastic behaviour of the blade in forward flight recast

$$\begin{aligned}
 & - \left[ v' \Omega^2 \int_x^R \mu x dx \right]' - \mu \Omega^2 [v + e \cos(\theta + \Phi)] + \\
 & \left\{ [EI_z - \Delta K \sin^2(\theta + \Phi)] v'' + \frac{1}{2} \Delta K \sin 2(\theta + \Phi) w'' \right\} + \\
 & - \left[ \mu(e - e_A) \Omega^2 x \cos(\theta + \Phi) \right] - 2\mu \Omega \beta_{pc} \dot{w} + \mu \ddot{v} + \quad (1)
 \end{aligned}$$

$$\begin{aligned}
 & - 2\mu \Omega \left( v' \int_x^R \dot{v} dx \right)' - 2\mu \Omega \int_0^x (\dot{v} v' + \dot{w} w') dx + \\
 & - \mu e \ddot{\Phi} \sin \theta - 2\mu e \Omega (v' \cos \theta + w' \sin \theta) + \\
 & - 2\Omega (\mu e \dot{v} \cos \theta)' = L_v \\
 & - \left[ w' \Omega^2 \int_x^R \mu x dx \right]' + \mu \Omega^2 \beta_{pc} x + \mu e \ddot{\Phi} \cos \theta + \\
 & \left\{ [EI_y - \Delta K \sin^2(\theta + \Phi)] w'' + \frac{1}{2} \Delta K \sin 2(\theta + \Phi) v'' \right\} + \\
 & - \left[ \mu(e - e_A) \Omega^2 x \sin(\theta + \Phi) \right] + 2\mu \Omega \beta_{pc} \dot{v} + \mu \ddot{w} + \quad (2)
 \end{aligned}$$

$$\begin{aligned}
 & - 2\mu \Omega \left( w' \int_x^R \dot{w} dx \right)' - 2\Omega (\mu e \dot{v} \sin \theta)' = L_w + F_w^{act} \\
 & - k_A \Omega^2 \left[ (\theta + \Phi)' \int_x^R \mu x dx \right]' + \mu e \Omega^2 \beta_{pc} x \cos \theta + \\
 & \Delta k \left[ v'' w'' \cos 2\theta + (w'^2 - v'^2) \frac{\sin 2\theta}{2} \right] - (GJ \Phi')' + \quad (3) \\
 & \mu \Omega^2 \Phi (k_{m_2}^2 - k_{m_1}^2) \cos 2\theta + \mu e \ddot{w} \cos \theta + \mu k_m^2 \ddot{\Phi} + \\
 & \mu e \Omega^2 x (w' \cos \theta - v' \sin \theta) - \mu e (\ddot{v} - \Omega^2 v) \sin \theta + \\
 & \mu \Omega^2 (k_{m_2}^2 - k_{m_1}^2) \cos \theta \sin \theta + \\
 & - e_A \Omega^2 (w'^2 \cos \theta - v'^2 \sin \theta) \int_x^R \mu x dx = M_\Phi + M_\Phi^{act}
 \end{aligned}$$

where  $\Omega$  is the rotor angular velocity whilst the unknowns are the displacements of the elastic axis tangent (lead-lag,  $v$ ) and orthogonal (flap,  $w$ ) to the surface defined by the pre-cone, as well as the cross-section torsion,  $\Phi$ , around it. Bending and torsional stiffnesses are  $EI_z$ ,  $EI_y$  and  $GJ$ , respectively,  $\Delta k = EI_z - EI_y$ ,  $\mu$  is the blade mass for unit length and  $x$  the spanwise position. In addition,  $k_{m_1}$ ,  $k_{m_2}$  are the principal mass radii of gyration,  $k_m^2 = k_{m_1}^2 - k_{m_2}^2$ ,  $\mu k_m^2$  the torsional mass moment of inertia,  $k_A$  the blade cross-section polar radius of gyration,  $\beta_{pc}$  the pre-cone angle,  $e$  the offset between the center of mass and the elastic axis whereas  $e_A$  the tension axis offset from the elastic axis. The blade mass for unit length takes into account for the concentrated masses located spanwise, i.e.,

$$\mu = \mu_b + \mu_k \delta(x - x_k)$$

where  $\mu_b$  denotes mass for unit length related to the basic blade and  $\mu_k$  is the  $k$ -th concentrated mass located at  $x_k$ . Forcing terms in equations (1)-(3), are the sum of actuation loads ( $F_w^{act}$  and  $M_\Phi^{act}$ ) and sectional

aerodynamic forces ( $L_v, L_w$  and  $M_\phi$ ). Following the description of the smart system given above, and observing that the SMA device is switched off, actuation loads arise from the localized bending moments due to the action of eccentric masses, that is

$$F_w^{act} = \Omega^2 \frac{\hat{t}}{2} [m_1 \delta'(x-x_1)x_1 + m_2 \delta'(x-x_2)x_2 + M \delta'(x-x_T)x_T]$$

$$M_\phi^{act} = \Omega^2 \frac{\hat{t}}{2} [m_1 \delta'(x-x_1)x_1 v'_1 + m_2 \delta'(x-x_2)x_2 v'_2 + M \delta'(x-x_T)x_T v'_T]$$

where  $M$  is the tip mass,  $\hat{t}$  denotes a portion of the cross-section thickness ( $\hat{t}=0$  only if masses stay on the elastic axis),  $v'_k$  is the lag-bending slope at  $x_k$  and  $\delta$  the Dirac delta function. Lagwise/flapwise loads  $L_v, L_w$  and the pitching moment  $M_\phi$  about the elastic center, are modelled through the quasi-steady approximation of the Greenberg 2D theory, [11] integrated with a wake-inflow at the rotor disk given by the free-wake boundary integral equation aerodynamic solver described in Ref. [12] (see also Ref. [13] for a more detailed description of the blade aeroelastic model applied).

### B. COUPLED TRIM ANALYSIS

The coupled trim analysis involves simultaneous solution of vehicle equilibrium equations and blade steady periodic aeroelastic response. The corresponding iterative procedure starts with a trim/aeroelastic solution using a linear wake inflow. It yields an initial guess for pitch controls setting and blade deformation that is used as input in a free-wake aerodynamic solver which, in turn, gives back a wake inflow to be used in the trim/aeroelastic step, until convergence is reached.

The steady periodic aeroelastic response is obtained by applying the Gal rkin approach for the space discretization and the harmonic balance method for the time integration [13]. In details, the blade elastic displacements are expressed in terms of the following series of generalized coordinates and shape functions

$$v(x,t) = \sum_{j=1}^N V_j(t) \Psi_j(x)$$

$$w(x,t) = \sum_{j=1}^N W_j(t) \Psi_j(x)$$

$$\Phi(x,t) = \sum_{j=1}^N \Phi_j(t) \theta_j(x)$$

where  $\Psi_j$  and  $\theta_j$  are bending and torsion natural modes of vibration of a non-rotating uniform cantilever beam, respectively. Then the projection of the blade dynamics equations onto the shape functions yields a set of  $3N$  nonlinear, nonhomogeneous, ordinary time differential equations in terms of modal generalized coordinates  $V_j, W_j$  and  $\Phi_j$ . The time integration is performed through a harmonic-balance procedure which, under the assumption of steady periodic response, provides the blade Lagrangean coordinates in terms of the Fourier coefficients obtained as solution of a set of algebraic equations [13].

### C. STABILITY ANALYSIS

Once the steady periodic blade response has been determined, stability analysis is accomplished. The first step of this procedure consists of deriving the small perturbation equations for the Lagrangean coordinates through the superposition of the steady periodic equilibrium configuration and small unsteady perturbations, i.e., assuming

$$V_j(t) = V_{0j}(t) + \Delta V_j(t)$$

$$W_j(t) = W_{0j}(t) + \Delta W_j(t)$$

$$\Phi_j(t) = \Phi_{0j}(t) + \Delta \Phi_j(t)$$

with  $V_{0j}, W_{0j}$  and  $\Phi_{0j}$  denoting the solution from the previous harmonic balance analysis. Then, the linearization of the resulting time differential equations yields the following set of homogenous equations for blade perturbations

$$\mathbf{M}\ddot{\mathbf{x}} + \mathbf{C}(t)\dot{\mathbf{x}} + \mathbf{K}(t)\mathbf{x} = \mathbf{0}$$

where the time-periodic matrices depend on  $V_{0j}$ ,  $W_{0j}$ ,  $\Phi_{0j}$  and  $\mathbf{x}^T = [\Delta V_j, \Delta W_j, \Delta \Phi_j]$ . Finally, the stability may be examined either through the application of the Floquet theory or by introducing the multiblade coordinate transformation and then performing a standard eigenvalue analysis.

**4. NUMERICAL RESULTS**

In this section the aeromechanical behaviour of the non-actuated smart rotor is investigated in forward flight where the blade tip morphing is not needed for BVI noise alleviation. Due to the additional masses included in the blade, the presence of the smart system might be no more compatible with an acceptable aeroelastic response of the blade. Thus, in the following, the smart rotor performance are compared with the baseline rotor in terms of trim control settings, vibratory hub loads and aeroelastic stability. The baseline rotor herein examined is a four-bladed hingeless Bo105-type model, with NACA 0015 cross sections and rotational speed equal to  $44.4 \text{ rad/s}$  (see Ref. [5] for details). The architecture of smart actuator is characterized by the additional masses  $m_1 = m_2 = 0.39 \text{ kg}$  located at  $x = 0.92R$  and  $x = 0.97R$ , respectively, and  $M = 0.4 \text{ kg}$  at the blade tip, coming from the investigation carried out in [6] for the hovering flight. The analysis is performed for a low-speed forward flight with advance ratio  $\mu = 0.15$  and for a medium-speed forward flight with advance ratio  $\mu = 0.25$ .

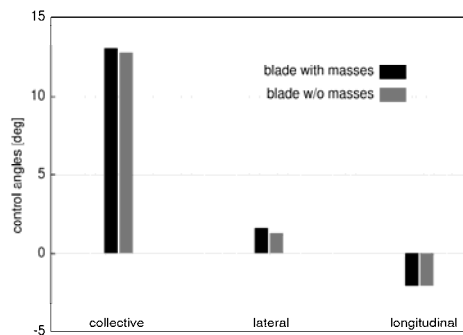


Fig. 5 Pitch control settings at  $\mu=0.15$

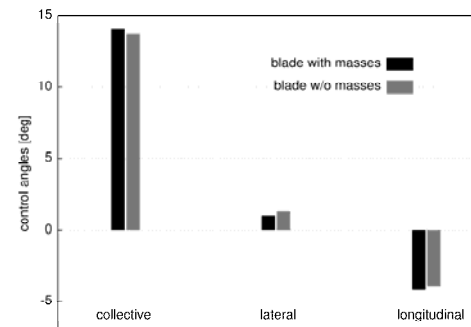


Fig. 6 Pitch control settings at  $\mu=0.25$

First, results in terms of propulsive trim, that is pitch control settings, are discussed. Trim procedure is here performed with the constraint that the total thrust must be equal to 25000N and pitching and rolling hub moments equal to 10Nm. Figure 5 depicts collective and cyclic pitch angles evaluated to trim the flight at  $\mu = 0.15$  with shaft angle equal to  $2^\circ$ , with and without the additional masses. The same kind of results are presented in Figure 6 for the flight at advance ratio  $\mu = 0.25$  and shaft angle equal to  $4^\circ$ . As shown, the inclusion of the smart system affects in an almost negligible way the trim control settings, both for low-speed and for medium-speed forward flight.

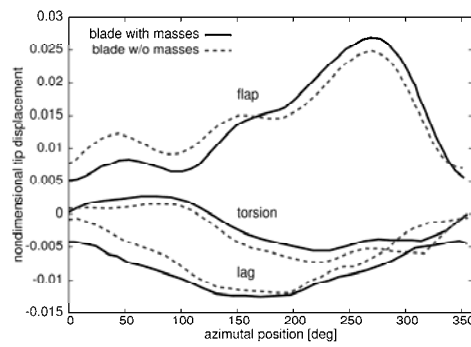


Fig. 7 Blade tip deflections at  $\mu=0.15$

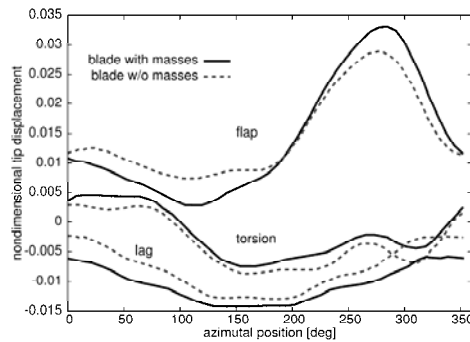


Fig. 8 Blade tip deflections at  $\mu=0.25$

Next, let us examine the comparison between the aeroelastic responses of baseline and smart rotor corresponding to the control settings shown above. Figures 7 and 8 depict the comparisons between the blade tip deflections experienced by the baseline blade and those experienced by the smart blade, respectively for  $\mu = 0.15$  and  $\mu = 0.25$ . In both cases the presence of the additional masses does not alter significantly the blade torsion, while causes an increase of the mean value of the lag deflection and amplitude of the flap deflection. At  $\mu = 0.25$ , the increases of lag mean value and flap amplitude are equal to about the 30% of the respective baseline values. For both advance ratios the introduction of the additional masses does not produce any phase shift of the displacements and this implies that the modifications in the natural frequencies of vibration do not cause first mode resonances.

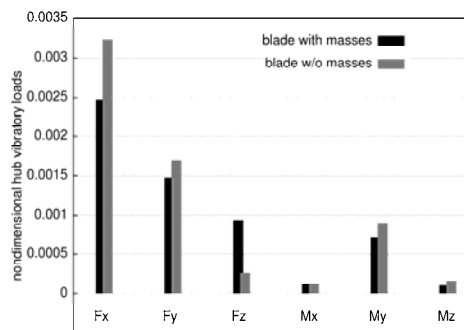


Fig. 9 4/ rev hub loads at  $\mu=0.15$

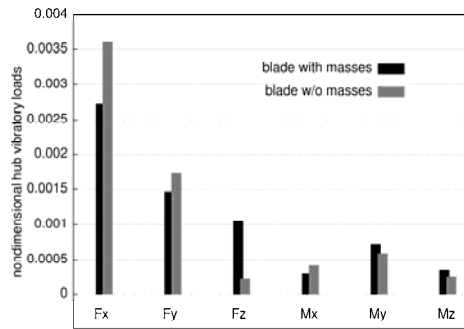


Fig. 10 4/ rev hub loads at  $\mu=0.25$

Table 1. Lowest nondimensional damping at  $\mu=0.15$

Linear inflow		Free-wake inflow	
without masses	with mass	without masses	with mass
-0.73	-0.43	-1.69	-0.91
-2.02	-1.69	-2.29	-1.81
-3.66	-3.70	-3.79	-3.77

Table 2. Lowest nondimensional damping at  $\mu=0.25$

Linear inflow		Free-wake inflow	
without masses	with mass	without masses	with mass
-0.78	-0.44	-1.80	-1.02
-2.04	-1.66	-2.00	-1.60
-3.60	-3.76	-3.81	-3.75

The differences in blade deflections affect the vibrating hub loads as illustrated in Figures 9 and 10. In particular, the inclusion of the additional masses causes some reduction of the vibrating in-plane forces, but a high increase of the out-of-plane vibrating force that turns out to be four times greater than the baseline value. However, the baseline out-of-plane force is strongly lower than the corresponding in-plane forces and hence, although increased, the one generated by the smart blade remains far from being critical. The vibratory hub moments are only slightly influenced by the presence of the smart system. Finally, the aeroelastic stability of baseline and smart rotors is analyzed by perturbing the periodic responses presented above. For this study a static wake inflow obtained both from an analytical linear model and through a free-wake solver has been used. Outcomes are highlighted in Tables 1 and 2 where the three lowest damping are given for  $\mu = 0.15$  and  $\mu = 0.25$ , respectively. As shown, the inclusion of additional masses causes a slight decrease of the critical damping for both advance ratios which, however, remain far from the stability boundary. This behaviour is observed using both wake inflow models, with the linear inflow predicting lower values of damping both for the baseline and for the smart blade.

### 5. CONCLUSIONS

In this paper the aeroelastic behaviour in forward flight of a smart blade has been investigated. The smart system included in the blade was proven to be effective in morphing the tip region so as to get an anhedral shape that is convenient in reducing BVI effects. The study presented here has been motivated by the fact that such device requires the presence of a set of concentrated masses located near the tip region that may negatively affect the aeroelastic response, hub loads and stability of the blade. The results obtained show that the influence of the smart device on the aeroelastic behaviour of the blade is acceptable: trim control settings and elastic response are only slightly affected by the introduction of the masses, whereas hub loads and stability margins are more influenced but remain in the range of the admissible values. Therefore the presence of the smart system is compatible with the requested aeromechanical performance of the rotor and thus the preliminary feasibility of its application on helicopters is demonstrated, at least from the aeroelastic standpoint.

### ACKNOWLEDGEMENTS

The authors wish to thank the Italian Aerospace Research Center (CIRA) where the concept of the smart actuator has been developed for the first time within the activities of the european project FriendCopter.

### REFERENCES

- [1] W. Johnson, Helicopter Theory.,Princeton University Press, 1980.
- [2] R.W.Prouty , Even More Helicopter Aerodynamics. Phillips Pub. Co.,1983.
- [3] C.Tung and S. Lee, "Evaluation of hover prediction codes", in Proceedings of the 50th Annual of the Am. Hel.Soc., Washington (DC),May 1994.
- [4] C.Testa, S.Leone, S.Ameduri and A.Concilio, "Feasibility study on rotorcraft blade morphing in hovering", in Proc.Proceedings of the International Symposium on Smart Structures and Materials, San Diego (CA), March 2005.
- [5] C.Testa, S.Leone, S.Ameduri and A.Concilio, "A feasibility study on the behaviour of a helicopter smart blade aimed at blade tip morphing", Journal of Theoretical and Applied Mechanics, vol.47 no.4,pp.897-921,2009.
- [6] C.Testa, S.Leone, J.Serafini and M.Gennaretti, "Aeroelastic investigation of hingeless helicopter blades with integrated smart morphing actuator", in Proc. Proceedings of European Rotorcraft Forum, Maastricht (The Netherlands), September 2006.
- [7] F.C.W.R. Spletstoesser, G.Niels and D. Papanikas, "Experimental results of the European helinoise aeroacoustic rotor test in the dnw", in Proc. Proceedings of the 19th European Rotorcraft Forum, Cernobbio (Italy), September 1993.
- [8] D.Hodge and E.Dowell, "Nonlinear equation for the elastic bending and torsion of twisted nonuniform rotor blades", NASA, NASA Technical Note TN D-7818,1974.
- [9] G. Bernardini, J.Serafini, M. Molica Colella and M.Gennaretti, "Fully coupled structural-unsteady aerodynamics modelling for aeroelastic response of rotorcraft", in Proc. Proceedings of 37th ERF, 13-15/9/2011 2011.
- [10] G. Bernardini, J.Serafini, M. Molica Colella and M.Gennaretti, "Analysis of a structural-aerodynamic full coupled formulation for aeroelastic response of rotorcraft", Aerospace Science and Technolog,2013. [Online]. Available: <http://dx.medra.org/10.1016/j.ast.2013.03.002>
- [11] J.Greenberg, "Airfoil in sinusoidal motion in a pulsing stream", NACA, NACA Technical Note 1326,1947.
- [12] M.Gennaretti and G.Bernardini, "A novel potential-flow boundary integral formulation for helicopter rotors in bvi conditions", in Proc. Proceedings of the 11th AIAA/CEAS Aeroacoustics Conference, Monterey (CA), May 2005.
- [13] M.Gennaretti and G.Bernardini, "Aeroelastic response of helicopter rotors using a 3-d un steady aerodynamic solver", The Aeronautical Journal, vol.110,pp.793-801,2006.